JMEPEG (2019) 28:2892–2902
https://doi.org/10.1007/s11665-019-04044-9

1059-9495/$19.00

Effect of Ca and Sm Combined Addition on the Microstructure and Elevated-Temperature Mechanical Properties of Mg-6Al Alloys

Yanhong Chen, Liping Wang, Yicheng Feng, Erjun Guo, Sicong Zhao, and Lei Wang

(Submitted September 14, 2018; in revised form February 10, 2019; published online April 17, 2019)

In the present study, the microstructure and elevated-temperature mechanical properties of Mg-6Al, Mg-6Al-4Ca, Mg-6Al-4Sm and Mg-6Al-2Ca-2Sm alloys were investigated. The experimental results showed that the microstructure and elevated-temperature mechanical property of Mg-6Al alloy changed obviously with the different elements addition. By analyzing the results of optical microscope, x-ray diffraction analysis, scanning electron microscope, and transmission electron microscope, it could be determined that there was only $Mg_{17}Al_{12}$ phase in Mg-6Al alloy, there were Al_2Ca and $(Mg, Al)_2Ca$ phases in Mg-6Al-4Ca alloy, there were Al_2Sm and $Mg_{17}Al_{12}$ phases in Mg-6Al-4Sm alloy, and there were $(Mg, Al)_2Ca$, Al_2Ca and Al_2Sm phases in Mg-6Al-2Ca-2Sm alloy. In addition, the addition of alloying elements including Ca and Sm, especially the composite addition, could significantly improve the tensile properties of Mg-6Al alloy. Compared to Mg-6Al alloy, the tensile strengths of Mg-6Al-2Ca-2Sm alloy at 448, 473 and 498 K were enhanced by 50.32, 87.92, and 94.99%, respectively. Furthermore, when the stretching temperatures were 448 and 473 K, the fracture pattern of Mg-6Al-2Ca-2Sm alloy was the mixture of intergranular fracture and trans-crystalline fracture. However, when the stretching temperature was 498 K, the fracture pattern of Mg-6Al-2Ca-2Sm alloy was the intergranular fracture.

Keywords fracture morphology, mechanical property, Mg alloy, microstructure

1. Introduction

Nowadays, Mg-Al alloys have wide prospects in automotive, electronics, and military industry products because of their advantages of lower density, excellent thermal conductivity, and recyclability (Ref 1-7). However, the heat-resistant performance of Mg-Al alloys is poor and their working temperatures are limited at 393 K; therefore, the wide application of Mg-Al alloys has been greatly restricted (Ref 8, 9). Hence, improving the heat resistance of Mg-Al alloys has become one of the focuses in the current research.

Wu et al. (Ref 10, 11) found that the main reason for the poor heat resistance of Mg-Al alloys is the β-$Mg_{17}Al_{12}$ phase, which was precipitated in the grain boundary. The β-$Mg_{17}Al_{12}$ phase softened at elevated temperature and lost the effect of inhibiting grain boundary slip. Hence, it made the Mg-Al alloys more prone to grain boundary sliding at elevated temperatures. Adding such elements as rare earth (RE) or alkaline earth to the alloy can improve its heat resistance (Ref 12-17). Zhang et al. (Ref 18) studied the effect of Nd elements on the microstructure of the as-cast Mg-4Al alloy. The research results showed that the Al elements in Mg-4Al alloy could combine preferentially with elemental Nd to form Al_2Nd and $Al_{11}Nd_3$ phases that had high thermostabilities. This inhibited the combination of Al and Mg elements and effectively prevented the precipitation of the β-$Mg_{17}Al_{12}$ phase. Furthermore, the study also found that, upon increasing the Nd content, the grain size of the alloy decreased remarkably. However, the price of the RE elements is relatively high and the addition of high RE content into the alloy greatly increased the production cost. As a relatively inexpensive element, the alkaline earth element Ca was very popular in the study of Mg-Al alloy. Wang et al. (Ref 19) studied the effect of Ca on the microstructure of Mg-Al alloys. The study found that the alkaline earth element Ca also had the function of improving the microstructure of Mg-Al alloys. Similar to the RE elements, Ca elements would combine preferentially with Al elements to form an Al_2Ca phase that had high thermostability. Hence, the phenomenon in which Al elements combine with Mg to form the β-$Mg_{17}Al_{12}$ phase was inhibited.

It was found in some previous studies that combining the addition of elemental Sm and Mn or elemental Sm and Zn in Mg-Al alloys can effectively improve the properties. Yang et al. (Ref 20) studied the structure of the Mg-4Al-4Sm-0.3Mn alloy, and found Al_2Sm and $Al_{12}Sm_2Mn_5$ phases in the alloy having refined microstructure. The Al_2Sm phase consisted of multiple twins, with the plane serving as the twinning plane. Furthermore, many twins were extraordinarily different from normal ones, featuring a sandwiched structure with the filling being $Al_{12}Sm_2Mn_5$ bands. Xu et al. (Ref 21) studied the microstructure and mechanical properties of Mg-Al-Sm-Zn alloy and found Al_2Sm and Mg-Zn phases in the alloy. The microstructure and mechanical properties of this alloy were significantly improved compared to those of Mg-Al alloy.

Therefore, the affinity between Al and Sm or Ca elements is larger than that between Al and Mg elements. This could inhibit

Yanhong Chen, Liping Wang, Yicheng Feng, Erjun Guo, Sicong Zhao, and **Lei Wang**, School of Materials Science and Engineering, Harbin University of Science and Technology, Harbin 150040, China. Contact e-mail: fyc7806067@163.com.

the precipitation of the β-$Mg_{17}Al_{12}$ phase effectively, and formed an intermetallic phase with high thermostability. Hence, it is worth considering whether the Mg-Al alloys that were combined with the Ca and Sm elements added simultaneously have the characteristics of Mg-Al-Ca and Mg-Al-Sm alloys, and whether the elevated-temperature mechanical properties of Mg-Al alloys can be further improved. However, there have been few studies about the Mg-Al-Ca-Sm alloys. Therefore, it is important to study the effect of combined Ca and Sm addition on Mg-Al alloys.

Hence, the aim of the present work was to study the effect of combined Ca and Sm addition on the microstructure and elevated-temperature mechanical properties of Mg-6Al alloys. By testing the microstructure, precipitated phase, phase distribution, and elevated-temperature tensile strength, the strengthening mechanism of Ca and Sm elements in Mg-6Al alloy was studied.

2. Experimental

2.1 Materials

In the present study, 4 wt.% Sm, 4 wt.% Ca and 2 wt.% Sm + 2 wt.% Ca were added into the Mg-6Al alloy, respectively. The experimental alloys were prepared by industrial pure magnesium (Mg ≥ 99.8%), industrial pure aluminum (Al ≥ 99.8%), Mg-30Ca master alloy (30% Ca) and Mg-30Sm master alloy (30% Sm). All the tested alloys were melted in steel crucible by using an electric resistant furnace. The pure magnesium and aluminum were melted at 993 K, and then, the Mg-Ca and Mg-Sm master alloys were melted at 1023 K. When all the master alloys were melted, the temperature was raised to 1043 K and held for 15 min, and then, the molten alloys were poured into a permanent mold (Φ60 × 150 mm). The actual compositions of all alloys are listed in Table 1, which were determined by inductively coupled plasma optical emission spectrometer (ICP-6300).

2.2 Microstructure and Elevated-Temperature Mechanical Properties Analysis

The samples for microstructure observation were cut from cast ingot with the same location and ground by using abrasive papers. Then the surfaces were polished and etched in a solution of 4 ml nitric acid and 96 ml ethyl alcohol. The microstructures of all samples were examined by optical microscope (GX71, OLYMPUS, Tokyo, Japan). The precipitated phases were examined by x-ray diffraction and scanning electron microscope. The x-ray diffraction (X'Pert-PRO) was equipped with Cu K_α at 40 kV and 40 mA. The scanning rate is 8°/min for 2θ ranging from 10° to 90°. The scanning electron microscope (Quanta 200, FEI, Eindhoven, The Netherlands) was equipped with an energy-dispersive x-ray spectrometer and transmission electron microscope (JEM-2100, 200 kV). The grain size of α-Mg phase was determined by the linear intercept method. The linear intercept method is drawing a straight line across at least five grains in the same OM micrograph. Taking measurements at least 10 times in each OM micrograph, the final average grain size was obtained by measuring five OM micrographs. The elevated-temperature mechanical properties of samples were conducted on the universal tensile testing machine (E44.304, MTS, America), equipped with an electronic furnace. The tensile properties were tested with a strain rate 0.5 mm/min at 448, 473, and 498 K, respectively. The sizes of tensile bars were 8 mm gauge length, 4 mm gauge width, and 2 mm gauge thickness, as shown in Fig. 1.

Table 1 Chemical composition of test alloys/wt.%

Alloy	Al	Ca	Sm	Mg
Mg-6Al	5.94	0	0	Bal.
Mg-6Al-4Ca	5.97	3.86	0	Bal.
Mg-6Al-4Sm	5.91	0	3.92	Bal.
Mg-6Al-2Ca-2Sm	5.89	1.91	1.95	Bal.

3. Results and Discussion

3.1 Microstructure Analysis

Figure 2 shows the optical microscope micrograph of Mg-6Al, Mg-6Al-4Ca, Mg-6Al-4Sm, and Mg-6Al-2Ca-2Sm alloys. As seen in Fig. 2, the microstructure of the Mg-6Al alloy changed obviously with the addition of different elements. The morphology of the α-Mg phase in Mg-6Al, Mg-6Al-4Sm, and Mg-6Al-2Ca-2Sm alloys is equiaxed. However, the morphology of the α-Mg phase in Mg-6Al-4Ca alloy is dendritic. Furthermore, all the precipitated phases in Mg-6Al and Mg-6Al-4Ca alloys are distributed in the boundary of grains. However, the precipitated phase in Mg-6Al-4Sm and Mg-6Al-2Ca-2Sm alloys is not only distributed in the grain boundary, but also in the grains.

In addition, the grain size of the α-Mg phase is also affected by the alloy composition. The grain sizes of Mg-6Al, Mg-6Al-4Ca, Mg-6Al-4Sm, and Mg-6Al-2Ca-2Sm alloys are shown in Fig. 3. The grain sizes of the α-Mg phase are 71.04 ± 1.36, 50.33 ± 2.58, 60.45 ± 2.25, and 41.90 ± 0.72 μm, which correspond to the alloys of Mg-6Al, Mg-6Al-4Ca, Mg-6Al-4Sm, and Mg-6Al-2Ca-2Sm, respectively. The grain size is the smallest with combined Ca and Sm addition in Mg-6Al alloy. This is because with combined Ca and Sm addition in Mg-6Al alloy, particle-like intermetallic phases were formed in the grain, and lamellar-like intermetallic phases were formed in the grain boundary. The theoretical calculation results reported by Qiu et al. (Ref 22) showed that the interfacial energy between Mg and Al_2Nd is very low (0.029 J/m^2), which promotes wetting. Therefore, the Al_2Nd particles can act as heterogeneous nucleating sites for the Mg matrix, which can act as grain

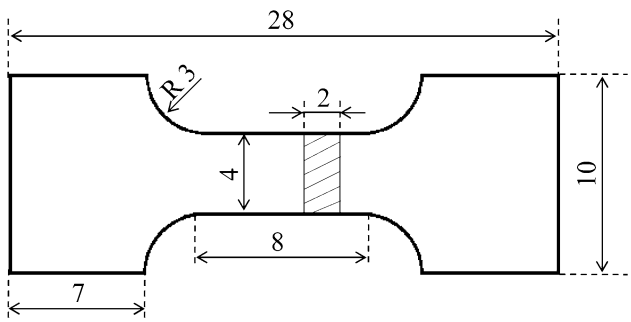

Fig. 1 The schematic of tensile bar

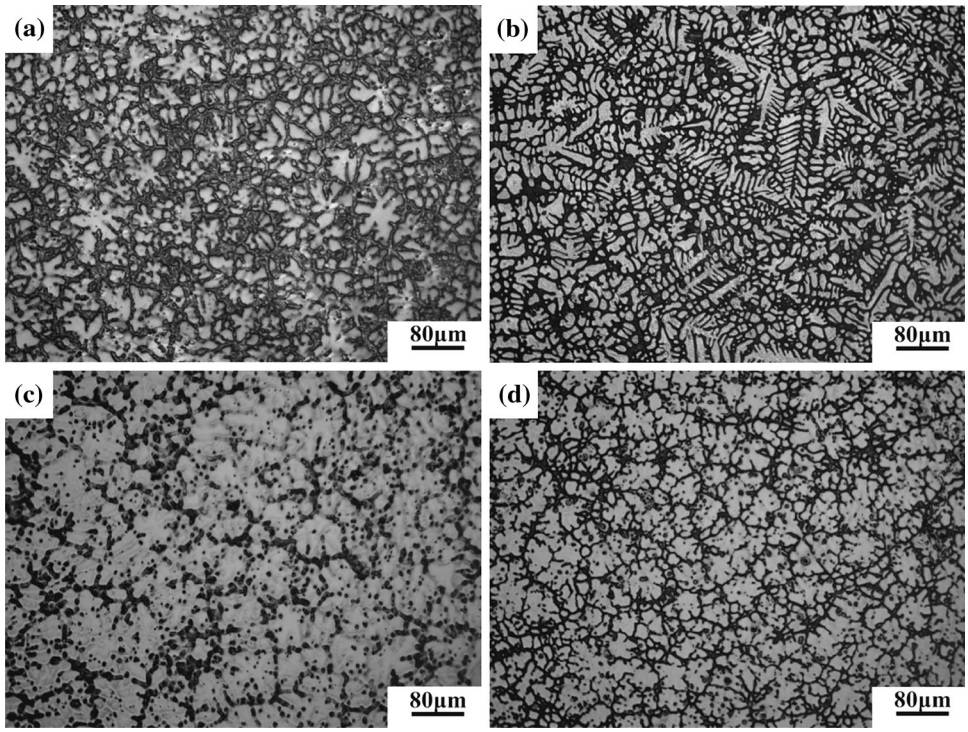

Fig. 2 The optical microscope micrograph of (a) Mg-6Al, (b) Mg-6Al-4Ca, (c) Mg-6Al-4Sm, and (d) Mg-6Al-2Ca-2Sm

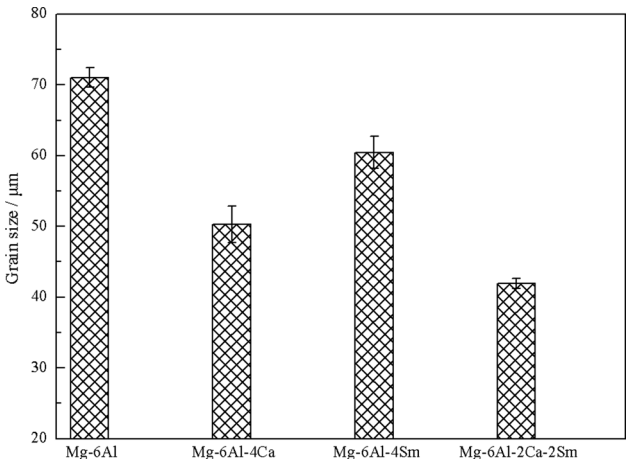

Fig. 3 The grain size of tested alloys

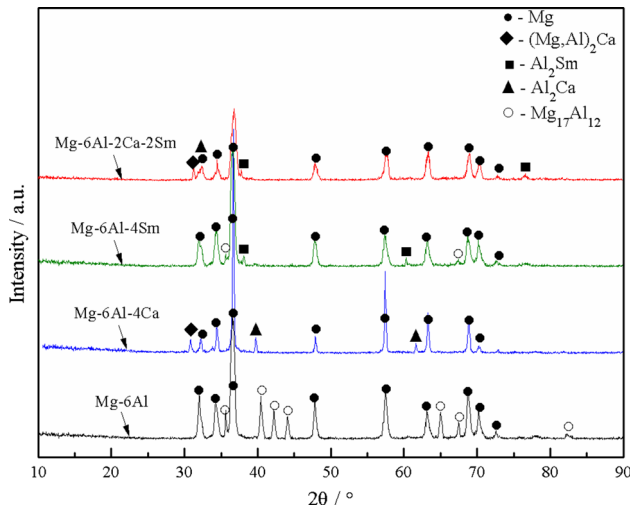

Fig. 4 The x-ray diffraction pattern for tested alloys

refiners for cast Mg alloys. Hence, the particle-like intermetallic phases that were formed in the grain acted as heterogeneous nucleation sites for α-Mg (Ref 23, 24). Furthermore, the lamellar-like intermetallic phases that were formed in the grain boundary hindered the continuous growth of grains. However, there is no particle structure phase in Mg-6Al-4Ca alloy and no lamellar-like phase in Mg-6Al-4Sm alloy. Hence, the grain size of Mg-6Al-2Ca-2Sm alloy is the smallest. This indicates that combined addition of Ca and Sm into Mg-6Al alloy can refine the grain size significantly.

To understand the precipitated phases in Mg-6Al, Mg-6Al-4Ca, Mg-6Al-4Sm, and Mg-6Al-2Ca-2Sm alloys, x-ray diffraction (XRD) analysis was performed, as shown in Fig. 4. There are obvious diffraction peaks of the β-$Mg_{17}Al_{12}$ phase in Mg-6Al and Mg-6Al-4Sm alloys. Furthermore, except for the β-$Mg_{17}Al_{12}$ phase, there is also a diffraction peak of the Al_2Sm phase in Mg-6Al-4Sm alloy, but there is no other precipitated phase in Mg-6Al alloy. In addition, there are obvious diffraction peaks of $(Mg, Al)_2Ca$ and Al_2Ca phases in Mg-6Al-4Ca and Mg-6Al-2Ca-2Sm alloys. In contrast, there is also a diffraction peak of the Al_2Sm phase in Mg-6Al-2Ca-2Sm alloy.

To verify further the precipitated phases in Mg-6Al, Mg-6Al-4Ca, Mg-6Al-4Sm, and Mg-6Al-2Ca-2Sm alloys, scanning electron microscopy (SEM) together with energy-dispersive x-ray spectroscopy (EDS) analysis and transmission electron spectroscopy (TEM) together with electron diffraction were performed. SEM micrographs of Mg-6Al, Mg-6Al-4Ca, Mg-6Al-4Sm, and Mg-6Al-2Ca-2Sm alloys are shown in Fig. 5. The morphologies of precipitated phases were different

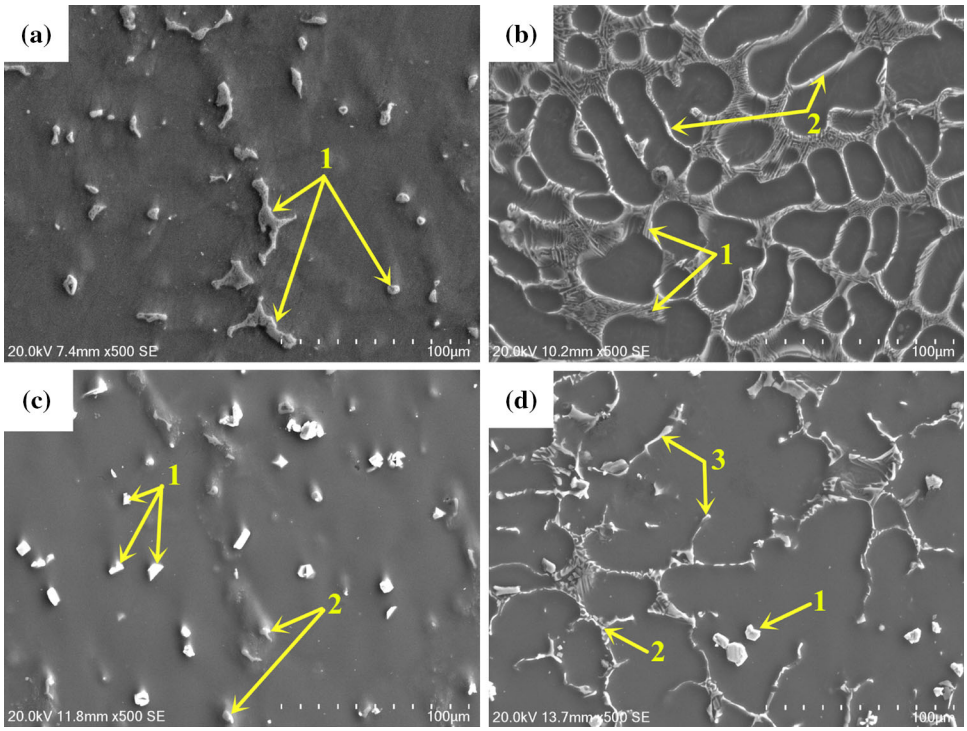

Fig. 5 SEM micrographs for: (a) Mg-6Al, (b) Mg-6Al-4Ca, (c) Mg-6Al-4Sm, and (d) Mg-6Al-2Ca-2Sm

with different elements additions. There was only a reticular structure phase in Mg-6Al alloy. However, when adding Ca or Sm separately in the alloy, there were lamella and fish-bone structure phases in Mg-6Al-4Ca alloy and particle and reticular structure phases in Mg-6Al-4Sm alloy. Furthermore, with combined addition of Ca and Sm, there were particle, lamella, and fish-bone structure phases in Mg-6Al-2Ca-2Sm alloy.

The EDS analysis results of the alloys are shown in Fig. 6. Analyzing the SEM micrographs, the reticular structure phase in Mg-6Al and Mg-6Al-4Sm alloys may be the β-$Mg_{17}Al_{12}$ phase. The particle structure phase in Mg-6Al-4Sm and Mg-6Al-2Ca-2Sm alloys may be the Al_2Sm phase. The lamella and fish-bone structure phases in Mg-6Al-4Ca and Mg-6Al-2Ca-2Sm alloys may be $(Mg, Al)_2Ca$ and Al_2Ca, respectively. When adding Sm separately in Mg-6Al alloy, although there was the Al_2Sm phase, which has high thermostability in the microstructure of Mg-6Al-4Sm alloy, there was still a small amount of the β-$Mg_{17}Al_{12}$ phase. However, when adding Ca separately or with combined addition of Ca and Sm in Mg-6Al alloy, there was no β-$Mg_{17}Al_{12}$ phase precipitated, and there were Al_2Sm, $(Mg, Al)_2Ca$, and Al_2Ca phases, which have high thermostability in Mg-6Al-2Ca-2Sm alloy (Ref 25, 26).

The representative TEM micrograph and diffraction patterns of the particle, fish-bone, lamella, and reticular structure phases are shown in Fig. 7. By calculating the interplanar spacing and angle in the diffraction patterns, it was determined that the particle structure phase is Al_2Sm, the fish-bone structure phase is Al_2Ca, the lamella structure phase is $(Mg, Al)_2Ca$, and the reticular structure phase is $Mg_{17}Al_{12}$. The results of TEM analysis are identical with SEM observations and EDS analysis. Hence, by analyzing comprehensively the experimental results of XRD, SEM, EDS, and TEM analysis, it can be determined that there is only $Mg_{17}Al_{12}$ phase in Mg-6Al alloy, there are Al_2Ca and $(Mg, Al)_2Ca$ phases in Mg-6Al-4Ca alloy, there are Al_2Sm and $Mg_{17}Al_{12}$ phases in Mg-6Al-4Sm alloy, and there are $(Mg, Al)_2Ca$, Al_2Ca, and Al_2Sm phases in Mg-6Al-2Ca-2Sm alloy. It also can be determined from the above experimental results that the varieties of precipitated phase that have high thermostability in Mg-6Al-2Ca-2Sm alloy are the maximum.

3.2 Elevated-Temperature Mechanical Properties Analysis

The tensile curve of Mg-6Al, Mg-6Al-4Ca, Mg-6Al-4Sm, and Mg-6Al-2Ca-2Sm alloys at 448, 473, and 498 K is shown in Fig. 8. The tensile strength of all tested alloys decreased with increasing experimental temperature. However, the elongation of all tested alloys increased with the experimental temperature. The tensile strength and elongation of these tested alloys are shown in Fig. 9. Figure 9(a) shows with 4 wt.% Ca in Mg-6Al alloy, and tensile strengths at 448, 473, and 498 K increased from 104.49 ± 7.21 to 136.03 ± 9.26 MPa, 71.54 ± 4.24 to 122.07 ± 7.21 MPa, and 61.06 ± 6.27 to 91.66 ± 7.54 MPa, respectively. The Ca-containing Mg-6Al-4Ca alloy exhibited relatively higher tensile strength at 448, 473, and 498 K than Mg-6Al alloy. Moreover, the Sm-containing Mg-6Al-4Sm alloy also exhibited higher tensile strength at 448, 473, and 498 K than Mg-6Al alloy. When containing 4 wt.% Sm in Mg-6Al alloy, the tensile strength at 448, 473, and 498 K increased from 104.49 ± 7.21 to 125.17 ± 5.24 MPa, 71.54 ± 4.24 to 111.74 ± 5.18 MPa, and 61.06 ± 6.27 to 102.56 ± 8.31 MPa, respectively. However, when the stretching temperatures were 448 and 473 K, the tensile strength of Mg-6Al-4Ca alloy was higher than that of Mg-6Al-4Sm alloy. On the contrary, when the stretching temperature was 498 K, the tensile strength of Mg-6Al-4Ca alloy was lower than that of Mg-6Al-4Sm alloy. The phenomenon is related to the precipitated phase in the two constituent alloys. The above microstructure analysis shows there are Al_2Ca and $(Mg, Al)_2Ca$ phases in Mg-6Al-4Ca alloy,

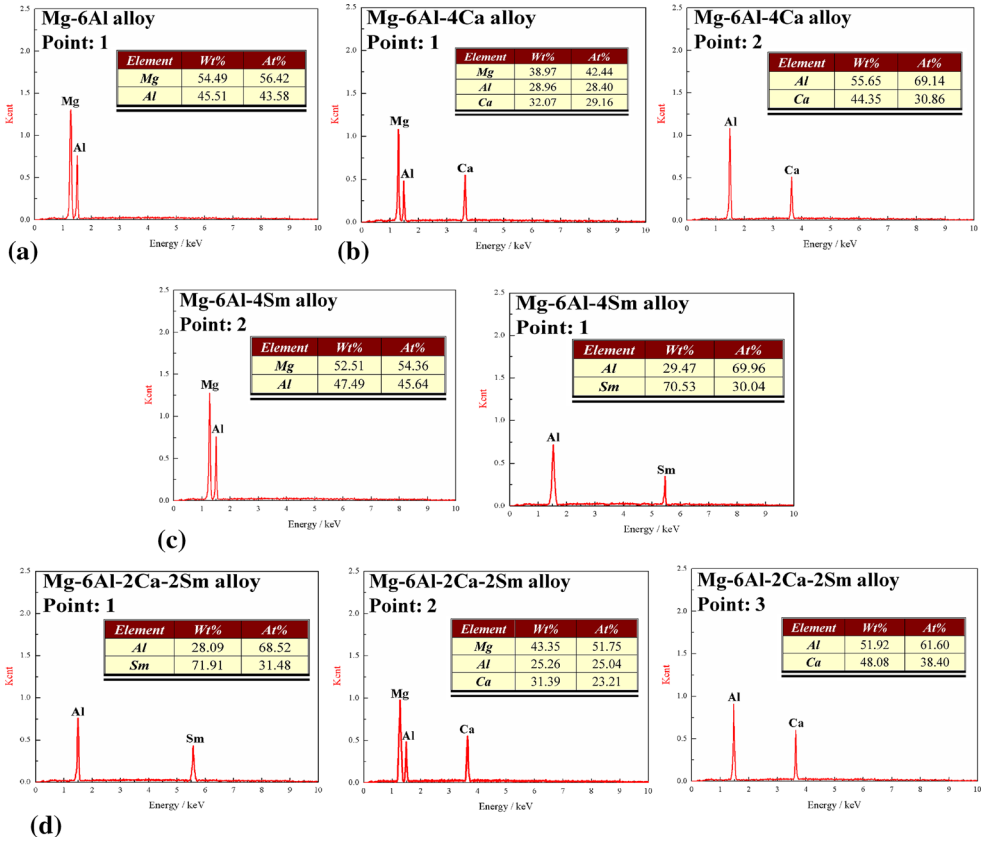

Fig. 6 EDS results from Fig. 5 for: (a) Mg-6Al, (b) Mg-6Al-4Ca, (c) Mg-6Al-4Sm, and (d) Mg-6Al-2Ca-2Sm

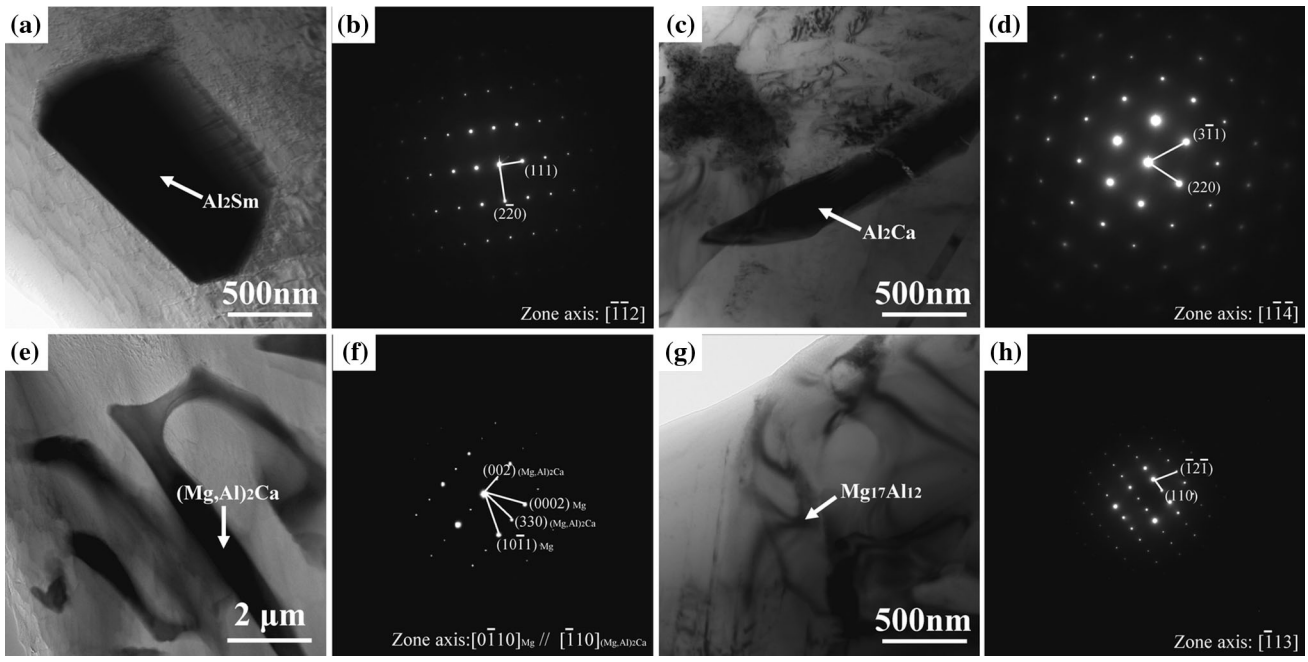

Fig. 7 TEM micrographs and diffraction patterns for: (a) particle structure phase, (b) fish-bone structure phase, (c) lamella structure phase, and (d) reticular structure phase

and there are Al_2Sm and $Mg_{17}Al_{12}$ phases in Mg-6Al-4Sm alloy. The Al_2Ca and (Mg, Al)$_2$Ca phases are distributed in the grain boundaries. Furthermore, the Al_2Sm phase is mainly distributed in the grains, and the $Mg_{17}Al_{12}$ phase is distributed in the grain boundaries. The Al_2Ca and (Mg, Al)$_2$Ca phases that distribute in the boundary of grains can play the role of grain boundary strengthening and improving the tensile strength of the alloy more effectively than the Al_2Sm phase, which mainly distributes

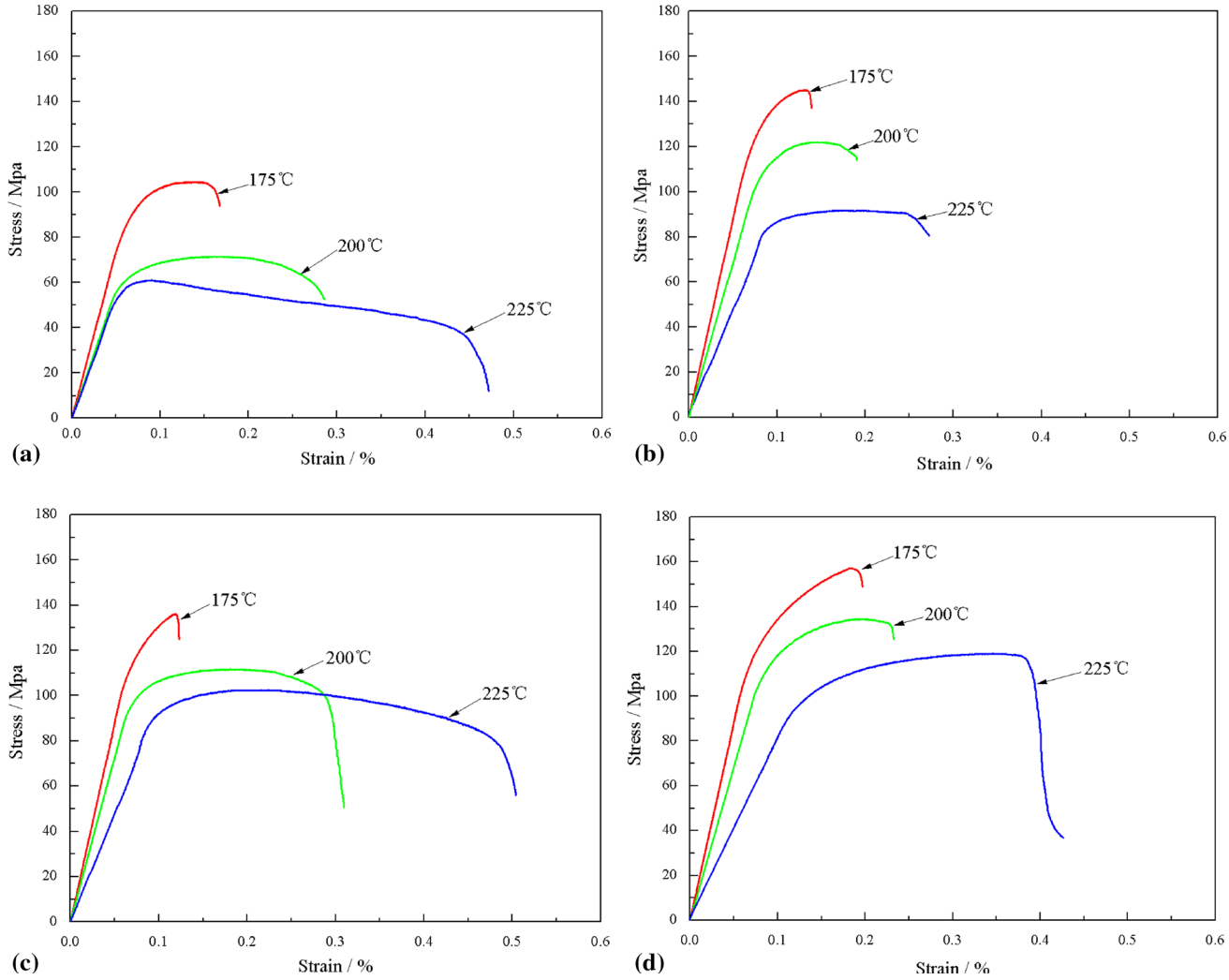

Fig. 8 The tensile curves of tested alloys at 448, 473, and 498 K. (a) Mg-6Al, (b) Mg-6Al-4Ca, (c) Mg-6Al-4Sm, and (d) Mg-6Al-2Ca-2Sm

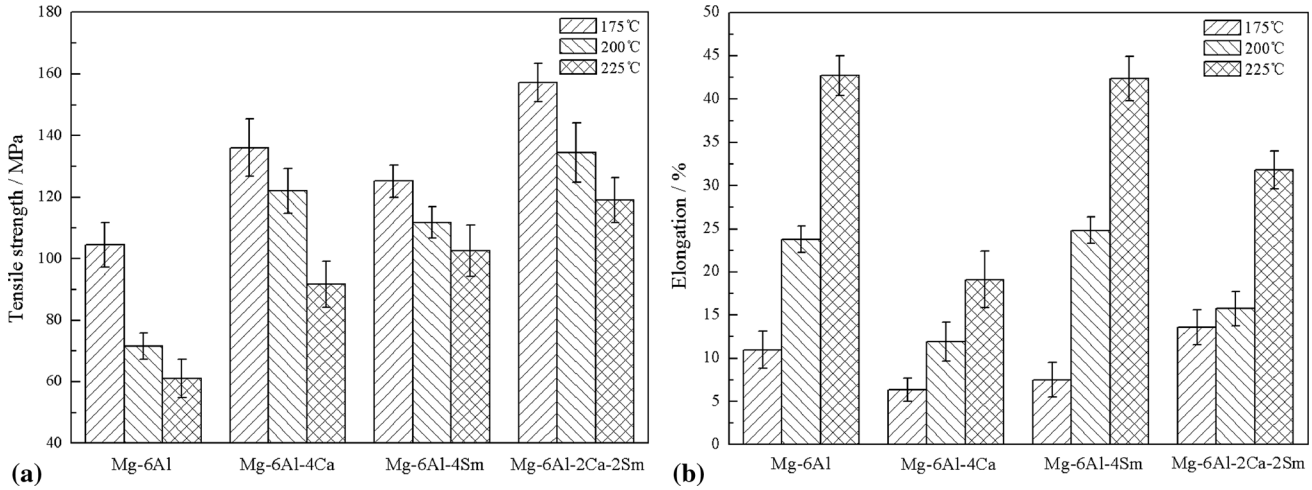

Fig. 9 The tensile strength and elongation of Mg-6Al, Mg-6Al-4Ca, Mg-6Al-4Sm, and Mg-6Al-2Ca-2Sm alloys at 448, 473, and 498 K

in grains. Moreover, when the stretching temperature rises, the $Mg_{17}Al_{12}$ phase softens and cannot strengthen the grain boundaries. However, when the stretching temperature is 498 K, the $(Mg, Al)_2Ca$ phase softens (Ref 27), while the Al_2Sm phase has high thermostability. Hence, when the stretching temperature is 498 K, the tensile strength of Mg-6Al-4Ca alloy is lower than that of Mg-6Al-4Sm alloy. Furthermore, with the combined addition of Ca and Sm in

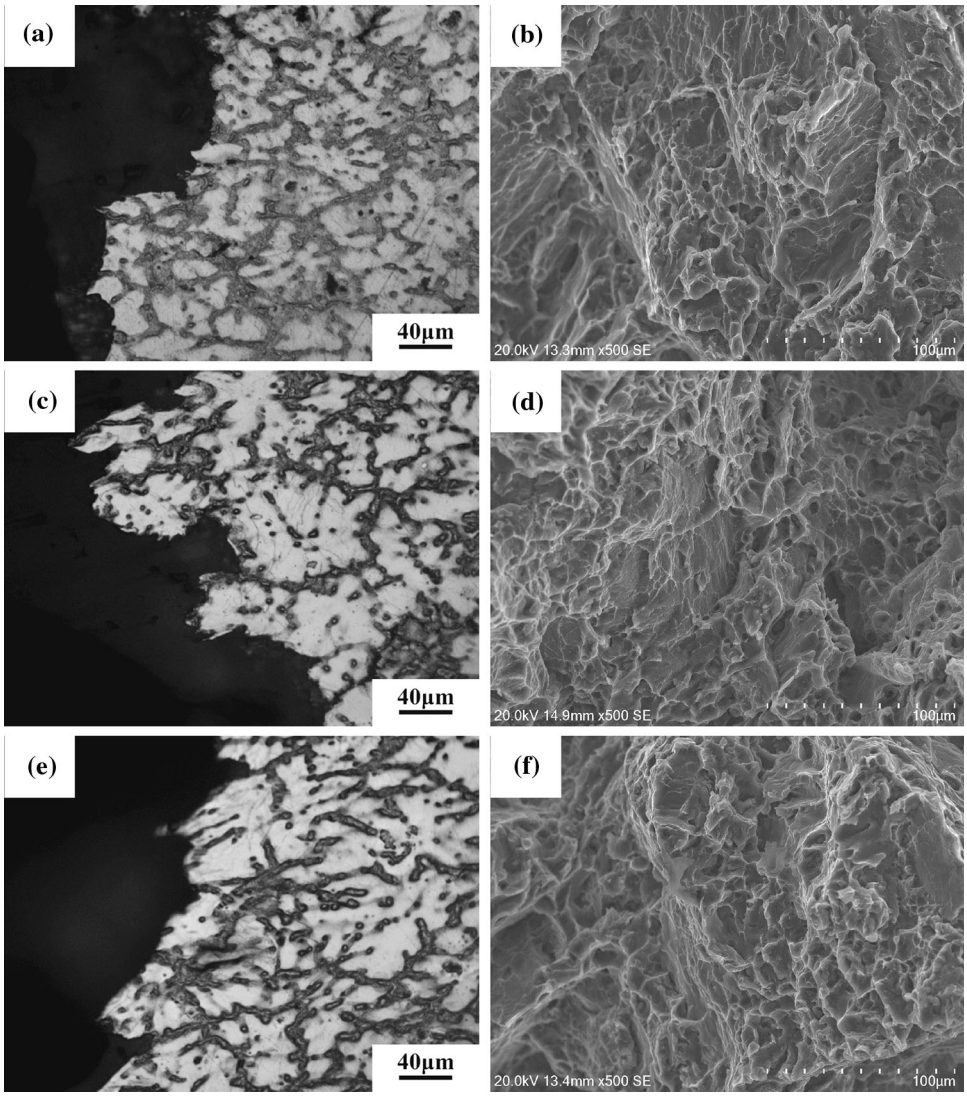

Fig. 10 The microstructure adjacent to the tensile fracture surfaces and the SEM of the tensile fracture surfaces of Mg-6Al alloy at 448, 473, and 498 K

Mg-6Al alloy, the tensile strength of Mg-6Al-2Ca-2Sm alloy at 448, 473, and 498 K is higher than that in Mg-6Al, Mg-6Al-4Ca and Mg-6Al-4Sm alloys. This is because there are Al_2Sm, Al_2Ca, and $(Mg, Al)_2Ca$ phases in Mg-6Al-2Ca-2Sm alloy. Not only do the Al_2Ca and $(Mg, Al)_2Ca$ phases play the role of grain boundary strengthening, but also the Al_2Sm phase, which is mainly distributed in grains, plays the role of heterogeneous nucleation and grain refinement (Ref 28). Hence, the addition of alloying elements including Ca and Sm, especially the composite addition, can significantly improve the tensile properties of Mg-6Al alloy. The tensile strength of Mg-6Al-2Ca-2Sm alloy at 448, 473, and 498 K is up to 157.07 ± 6.23, 134.44 ± 9.64, and 119.06 ± 7.28 MPa, respectively. Compared to Mg-6Al alloy, the tensile strengths of the alloy at 448, 473, and 498 K are enhanced by 50.32, 87.92, and 94.99%, respectively.

In addition, as seen in Fig. 9(b), the elongations of Mg-6Al and Mg-6Al-4Sm alloys are almost the same. The elongation observably increases with the experimental temperature. This phenomenon is in accordance with the movement of the non-base slip system. There is only the $Mg_{17}Al_{12}$ phase distributed in the grain boundary of Mg-6Al and Mg-6Al-4Sm alloys. When the stretching temperature rises, the $Mg_{17}Al_{12}$ phase softens, so it cannot play the role of grain boundary strengthening. As a result, under the action of external forces, the grains are more prone to displacement. However, with 4 wt.% Ca in Mg-6Al alloy, the elongation of Mg-6Al-4Ca alloy shows significant reduction. When the experimental temperatures are 448, 473, and 498 K, the elongation decreases from $10.96\% \pm 2.14\%$ to $6.37\% \pm 1.37\%$, $23.79\% \pm 1.58\%$ to $11.92\% \pm 2.26\%$, and $42.7\% \pm 2.32\%$ to $19.1\% \pm 3.28\%$, respectively. This is because there are Al_2Ca and $(Mg, Al)_2Ca$ phases in Mg-6Al-4Ca alloy, and the Ca phase belongs to the brittle phase. Furthermore, the Al_2Ca and $(Mg, Al)_2Ca$ phases distribute in the grain boundary of Mg-6Al-4Ca alloy, and they can play the role of grain boundary strengthening and inhibiting effectively the displacement between grains. Hence, the elongation of Mg-6Al-4Ca alloy is lower than those of Mg-6Al and Mg-6Al-4Sm alloys. Moreover, the elongation of Mg-6Al-2Ca-2Sm alloy is higher than that of Mg-6Al-4Ca alloy but lower than those of Mg-6Al and Mg-6Al-4Sm alloys.

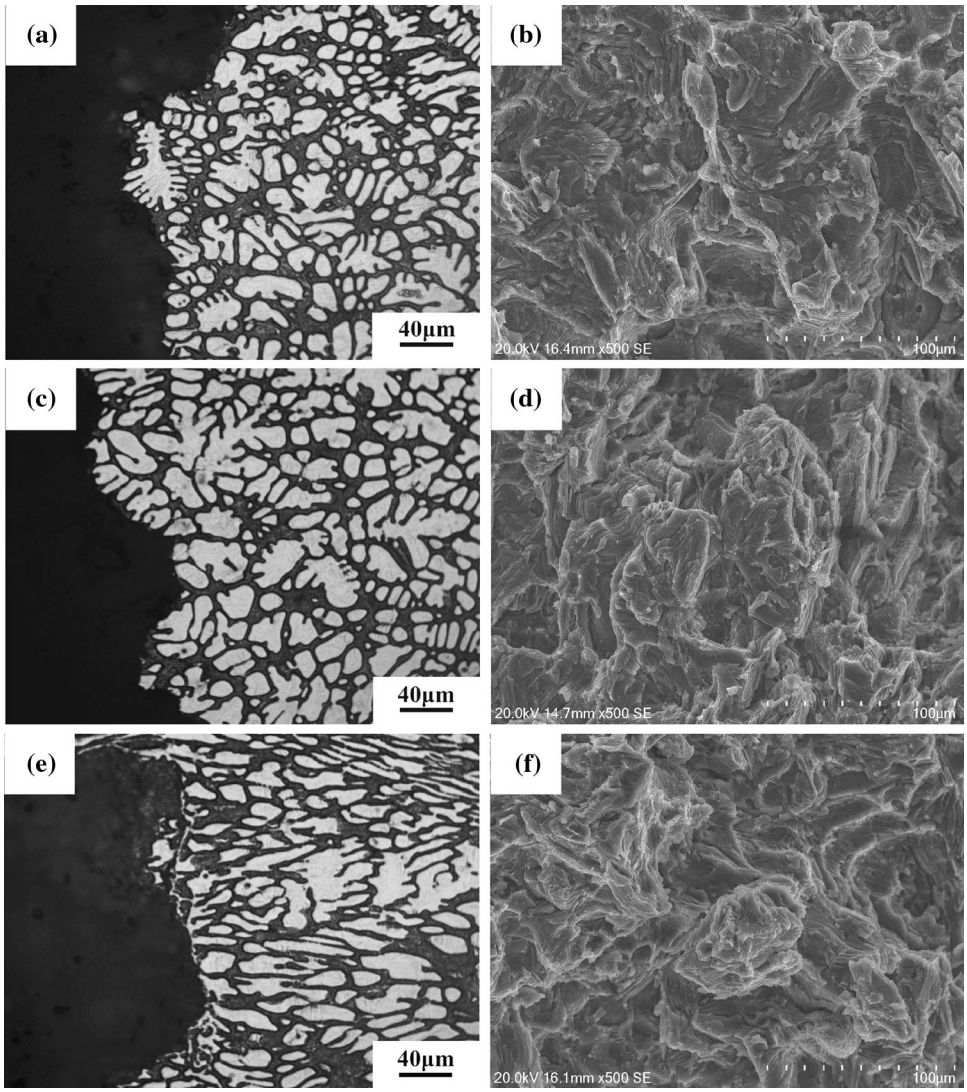

Fig. 11 The microstructure adjacent to the tensile fracture surfaces and the SEM of the tensile fracture surfaces of Mg-6Al-4Ca alloy at 448, 473, and 498 K

With Mg-6Al-4Ca alloy, Al_2Ca and $(Mg, Al)_2Ca$ phases that belong to the brittle phase distribute in the grain boundary of Mg-6Al-2Ca-2Sm alloy. However, there is also a particle structure Al_2Sm phase in the grains. The Al_2Sm particles are formed and act as heterogeneous nucleation sites for the α-Mg phase; thus, the grain size is refined. Hence, the elongation of Mg-6Al-2Ca-2Sm alloy is higher than that of Mg-6Al-4Ca alloy, but lower than those of Mg-6Al and Mg-6Al-4Sm alloys.

Figure 10-13 shows the microstructures adjacent to the tensile fracture surfaces and the SEM images of the tensile fracture surfaces of Mg-6Al, Mg-6Al-4Ca, Mg-6Al-4Sm, and Mg-6Al-2Ca-2Sm alloys at 448, 473, and 498 K. As shown by the microstructures adjacent to the tensile fracture surfaces in these figures, when the stretching temperature is 448 K, the fracture pattern of Mg-6Al alloy is a trans-crystalline fracture. However, when the stretching temperatures are 473 and 498 K, the fracture pattern of Mg-6Al alloy is intergranular fracture. Moreover, Fig. 10(b), (d), and (f) shows that the fracture morphology of Mg-6Al alloy at 448 K consists of a dispersed cleavage plane and a discontinuous tear ridge. However, when the stretching temperature was increased to 473 and 498 K, the fracture morphologies of Mg-6Al alloy consisted of a dispersed dimple region and continuous tear ridge. This also confirms that when the stretching temperature is 448 K, the fracture pattern of Mg-6Al alloy is a trans-crystalline fracture, and when the temperatures are 473 and 498 K, the fracture pattern is an intergranular fracture. This is because, when the stretching temperature is 448 K, the $Mg_{17}Al_{12}$ phase that distributes in the boundary of grains can strengthen the grain boundary. However, when the stretching temperature increases, the $Mg_{17}Al_{12}$ phase softens and becomes more likely to break.

As shown in Fig. 11(b), (d), and (f), the fracture morphologies of Mg-6Al-4Ca alloy at 448, 473, and 498 K consist of a dispersed cleavage plane and a discontinuous tear ridge. This indicates that the fracture patterns of Mg-6Al-4Ca alloy at 448, 473, and 498 K are both trans-crystalline fracture. Furthermore, as seen in Fig. 11(a), (c), and (e), when the stretching temperatures are 448 and 473 K, the microstructures of the Mg-6Al-4Ca alloy are essentially unchanged. However, when the stretching temperature is 498 K, the microstructure extends

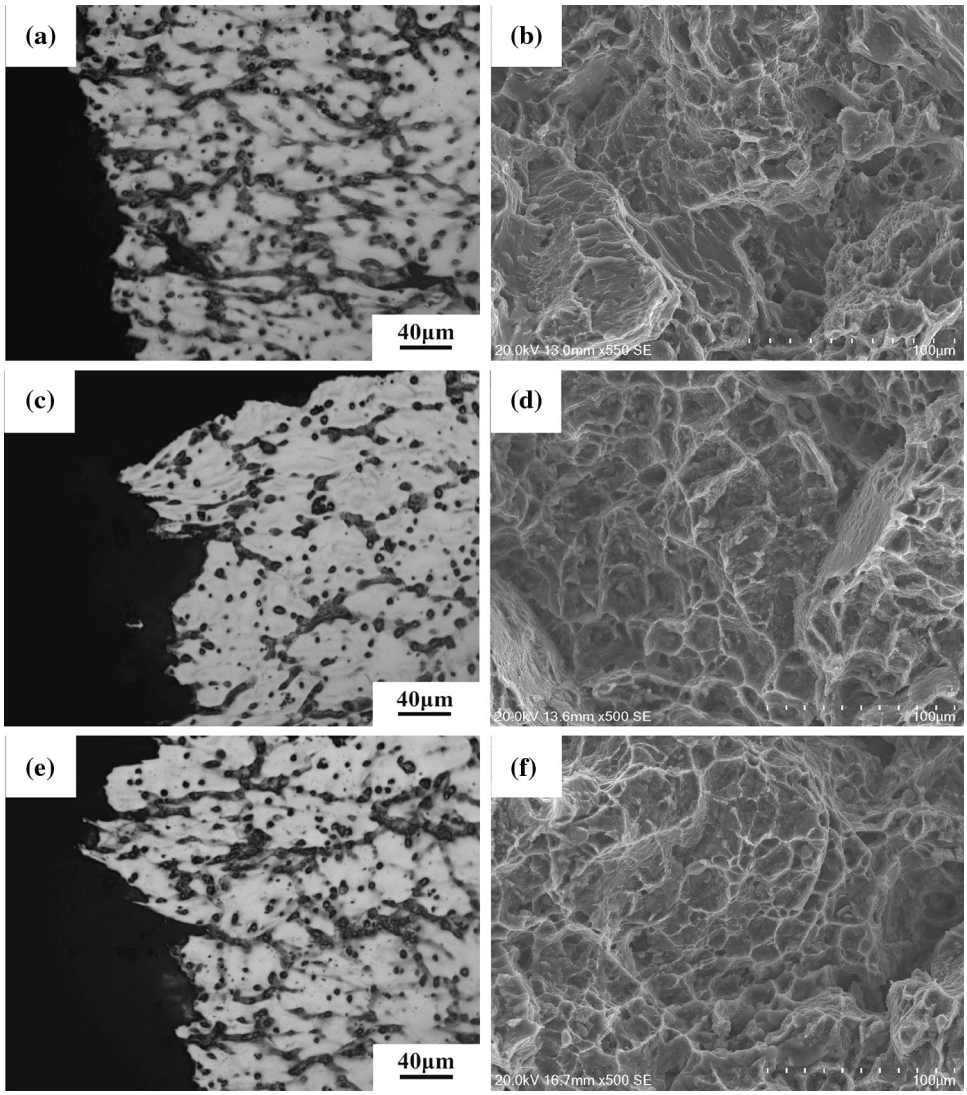

Fig. 12 The microstructure adjacent to the tensile fracture surfaces and the SEM of the tensile fracture surfaces of Mg-6Al-4Sm alloy at 448, 473, and 498 K

to the tensile direction. This is because, when the stretching temperature is 498 K, the $(Mg, Al)_2Ca$ phase that distributes in the boundary of grains softens, and it cannot strengthen the grain boundary effectively.

As shown in Fig. 12(b), (d), and (f), the fracture morphologies of Mg-6Al-4Sm alloy at 448, 473, and 498 K consist of a dispersed dimple region and continuous tear ridge. This indicates that the fracture patterns of Mg-6Al-4Sm alloy at 448, 473, and 498 K are both intergranular fracture. Furthermore, as seen in Fig. 12(a), (c), and (e), by increasing the stretching temperature, the microstructure of Mg-6Al-4Sm alloy extends a little to the tensile direction. This is because, when increasing the stretching temperature, the $Mg_{17}Al_{12}$ phase softens, but the Al_2Sm phase that mainly distributes in grains has high thermostability, and it can strengthen the grains.

As shown in Fig. 13(a) and (c), when the stretching temperatures are 448 and 473 K, there are cracks that extend perpendicularly to the tensile direction in Mg-6Al-2Ca-2Sm alloy. The lamella structure $(Mg, Al)_2Ca$ eutectic phase distributes in the boundary of grains. The stress concentration is formed when the dislocation accumulates at the grain boundary during stretching. When the stress is large enough, the crack forms easily at the interface between the eutectic phase and matrix (Ref 29). As the number of cracks increases, they connect with each other and cause the alloy to break. Figure 13(b) and (d) shows the SEM images of the tensile fracture surfaces of Mg-6Al-2Ca-2Sm alloy at 448 and 473 K. The fracture morphologies of the alloy at 448 and 473 K consist of dispersed cleavage plane and discontinuous tear ridge. Hence, when the stretching temperatures are 448 and 473 K, the fracture pattern of Mg-6Al-2Ca-2Sm alloy is the mixture of intergranular fracture and trans-crystalline fracture. However, when the stretching temperature is 498 K, the microstructure of Mg-6Al-2Ca-2Sm alloy extends in the tensile direction, as shown in Fig. 13(e). This is because, when the stretching temperature is 498 K, the $(Mg, Al)_2Ca$ phase that distributes in the boundary of grains softens, and it cannot strengthen the grain boundary effectively. Figure 13(f) shows that, when the stretching temperature is 498 K, the fracture morphology of the alloy consists of a dispersed dimple region

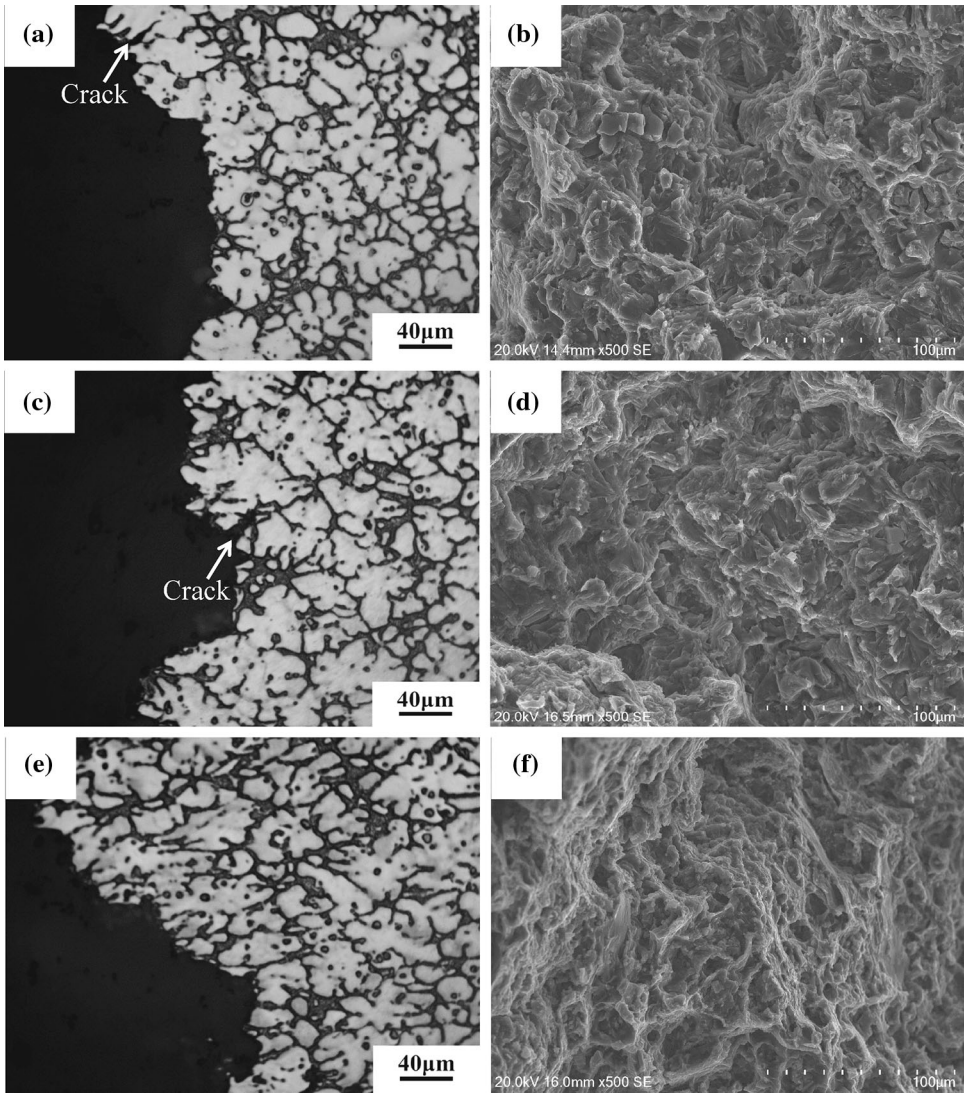

Fig. 13 The microstructure adjacent to the tensile fracture surfaces and the SEM of the tensile fracture surfaces of Mg-6Al-2Ca-2Sm alloy at 448, 473, and 498 K

and continuous tear ridge. Hence, when the stretching temperature is 498 K, the fracture pattern of Mg-6Al-2Ca-2Sm alloy is intergranular fracture.

4. Conclusion

1. By adding different elements, the precipitated phase in Mg-6Al alloy is also different. There is only $Mg_{17}Al_{12}$ phase in Mg-6Al alloy, there are Al_2Ca and $(Mg, Al)_2Ca$ phases in Mg-6Al-4Ca alloy, there are Al_2Sm and $Mg_{17}Al_{12}$ phases in Mg-6Al-4Sm alloy, and there are $(Mg, Al)_2Ca$, Al_2Ca and Al_2Sm phases in Mg-6Al-2Ca-2Sm alloy.
2. The addition of alloying elements including Ca and Sm, especially the composite addition, can significantly improve the tensile properties of Mg-6Al alloy. Compared to Mg-6Al alloy, the tensile strengths of Mg-6Al-2Ca-2Sm alloy at 448, 473, and 498 K are enhanced by 50.32, 87.92, and 94.99%, respectively. In the Mg-6Al-2Ca-2Sm alloy, not only the Al_2Ca and $(Mg, Al)_2Ca$ phases play the role of grain boundary strengthening, but also the Al_2Sm phase which is mainly distributed in the grains plays the role of heterogeneous nucleation and grain refinement.
3. When the stretching temperatures are 448 and 473 K, the fracture pattern of Mg-6Al-2Ca-2Sm alloy is the mixture by intergranular fracture and trans-crystalline fracture. When the stretching temperature is 498 K, the fracture pattern of Mg-6Al-2Ca-2Sm alloy is the intergranular fracture, the $(Mg, Al)_2Ca$ phase which is distributed in the boundary of grains will soften at 498 K, and it cannot strengthen the grain boundary effectively.

Acknowledgments

The authors gratefully acknowledge the financial support from the Heilongjiang Province Natural Science Foundation (No. E2018045).

References

1. B. Chen, J.X. Zheng, C.M. Yang, Y.X. Chen, S.C. Cao, Z.X. Zhao, X.L. Li, and C. Lu, Mechanical Properties and Deformation Mechanisms of Mg-Gd-Y-Zr Alloy at Cryogenic and Elevated Temperatures, *J. Mater. Eng. Perform.*, 2016, **26**, p 1–11
2. L.Q. Wu, R.Z. Wu, L.G. Hou, J.H. Zhang, J.F. Sun, and M.L. Zhang, Microstructure and Mechanical Properties of CNT-Reinforced AZ31 Matrix Composites Prepared Using Hot-Press Sintering, *J. Mater. Eng. Perform.*, 2017, **42**, p 1–6
3. C.Y. Zhao, X.H. Chen, F.S. Pan, S.Y. Gao, D. Zhao, and X.F. Liu, Effect of Sn Content on Strain Hardening Behavior of as-Extruded Mg-Sn Alloys, *Mat. Sci. Eng. A*, 2018, **713**, p 244–252
4. F. Li, X. Zeng, and G.J. Cao, Investigation of Microstructure Characteristics of the CVCDEed AZ31 Magnesium Alloy, *Mat. Sci. Eng. A*, 2015, **639**, p 395–401
5. K.K. Deng, J.Y. Shi, C.J. Wang, X.J. Wang, Y.W. Wu, K.B. Nie, and K. Wu, Microstructure and Strengthening Mechanism of Bimodal Size Particle Reinforced Magnesium Matrix Composite, *Compos. A Appl. Sci. Manuf.*, 2012, **43**, p 1280–1284
6. H.H. Yu, Y.C. Xin, M.Y. Wang, and Q. Liu, Hall-Petch Relationship in Mg Alloys: A Review, *J. Mater. Sci. Technol.*, 2018, **34**, p 248–256
7. G.Q. Li, J.H. Zhang, R.Z. Wu, Y. Feng, S.J. Liu, X.J. Wang, Y.F. Jiao, Q. Yang, and J. Meng, Development of High Mechanical Properties and Moderate Thermal Conductivity Cast Mg Alloy With Multiple RE Via Heat Treatment, *J. Mater. Sci. Technol.*, 2018, **34**, p 1076–1084
8. S. Zhu, M.A. Easton, T.B. Abbott, J.F. Nie, M.S. Dargusch, N. Hort, and M.A. Gibson, Evaluation of Magnesium Die-Casting Alloys for Elevated Temperature Applications: Microstructure, Tensile Properties, and Creep Resistance, *Metall. Mater. Trans. A*, 2015, **46**, p 3543–3554
9. B. Nami, S.G. Shabestari, H. Razavi, S. Mirdamadi, and S.M. Miresmaeili, Effect of Ca, RE Elements and Semi-Solid Processing on the Microstructure and Creep Properties of AZ91 Alloy, *Mat. Sci. Eng. A*, 2011, **528**, p 1261–1267
10. Y. Zhang, L. Yang, J. Dai, J. Ge, G. Guo, and Z. Liu, Effect of Ca and Sr on the Compressive Creep Behavior of Mg-4Al-RE Based Magnesium Alloys, *Mater. Des.*, 2014, **63**, p 439–445
11. V.G. Tkachenko, K.H. Kim, B.G. Moon, and A.S. Vovchok, Design and Microstructural Analysis of Magnesium Alloys for Dynamical Applications, *J. Mater. Sci.*, 2011, **46**, p 4880–4895
12. F. Wang, Y. Wang, P.L. Mao, B.Y. Yu, and Q.Y. Guo, Effects of Combined Addition of Y and Ca on Microstructure and Mechanical Properties of Die Casting AZ91 Alloy, *Trans. Nonferrous Met. Soc. China*, 2010, **20**, p S311–s317
13. Y. Terada, Y. Murata, and T. Sato, Life Assessment of Die-Cast Mg-5Al-1.7Ca Alloys Under Creep Service Conditions, *Mat. Sci. Eng. A*, 2014, **613**, p 136–140
14. J. Liu, W.X. Wang, S. Zhang, D.J. Zhang, and H.Y. Zhang, Effect of Gd-Ca Combined Additions on the Microstructure and Creep Properties of Mg-7Al-1Si Alloys, *J. Alloys Compd.*, 2015, **620**, p 74–79
15. J. Bai, Y.S. Sun, F. Xue, S. Xue, J. Qiang, and W.J. Tao, Effect of Extrusion on Microstructures, and Mechanical and Creep Properties of Mg-Al-Sr and Mg-Al-Sr-Ca Alloys, *Scripta Mater.*, 2006, **55**, p 1163–1166
16. Q. Yang, F.Q. Bu, X. Qiu, Y.D. Li, W.R. Li, W. Sun, X.J. Liu, and J. Meng, Strengthening Effect of Nano-Scale Precipitates in a Die-Cast Mg-4Al-5.6Sm-0.3Mn Alloy, *J. Alloys Compd.*, 2016, **665**, p 240–250
17. M.L. Su, J.H. Zhang, Y. Feng, Y.J. Bai, W. Wang, Z.W. Zhang, and F.C. Jiang, Al-Nd Intermetallic Phase Stability and Its Effects on Mechanical Properties and Corrosion Resistance of HPDC Mg-4Al-4Nd-0.2Mn Alloy, *J. Alloys Compd.*, 2017, **691**, p 634–643
18. J.H. Zhang, J. Wang, X. Qiu, D.P. Zhang, Z. Tian, X.D. Niu, D.X. Tang, and J. Meng, Effect of Nd on the Microstructure, Mechanical Properties and Corrosion Behavior of Die-Cast Mg-4Al-Based Alloy, *J. Alloys Compd.*, 2008, **464**, p 556–564
19. Q.D. Wang, W.Z. Chen, X.Q. Zeng, Y.Z. Lu, W.J. Ding, Y.P. Zhu, and X.P. Xu, Effects of Ca Addition on the Microstructure and Mechanical Properties of AZ91 Magnesium Alloy, *J. Mater. Sci.*, 2001, **36**, p 3035–3040
20. Q. Yang, K. Guan, X. Qiu, D.P. Zhang, S.H. Lv, F.Q. Bu, Y.Q. Zhang, X.J. Liu, and J. Meng, Structures of Al2Sm Phase in a High-Pressure Die-Cast Mg-4Al-4Sm-0.3Mn Alloy, *Mat. Sci. Eng. A*, 2016, **675**, p 396–402
21. G.L. Xu, X.L. Yuan, and L.B. Liu, Microstructure and Mechanical Property of Mg-Al-Zn-Sm Alloy and Its Thermodynamic Analysis, *Chin. J. Nonferrous Met.*, 2012, **22**, p 1255–1261
22. D. Qiu and M.X. Zhang, The Nucleation Crystallography and Wettability of Mg Grains On Active Al_2Y Inoculants In An Mg-10 wt.% Y Alloy, *J. Alloys Compd.*, 2014, **586**, p 39–44
23. L. Wang, Y.C. Feng, E.J. Guo, Y. Yang, Y.C. Chen, and L.P. Wang, Effect of Cooling Rate on the Grain Refinement of Mg-3Nd Alloys by Aluminum, *Int. J. Metalcast.*, 2018, https://doi.org/10.1007/s40962-018-0224-5
24. C.L. Wang, J.C. Dai, W.C. Liu, L. Zhang, and G.H. Wu, Effect of Al Additions on Grain Refinement and Mechanical Properties of Mg-Sm Alloys, *J. Alloys Compd.*, 2015, **620**, p 172–179
25. Y.F. Jiao, J.H. Zhang, L.L. He, M.L. Zhang, F.C. Jiang, W. Wang, L.M. Han, L.J. Xu, and R.Z. Wu, Al-RE Intermetallic Phase Stability and Effects on Corrosion Behavior in Cold-Chamber HPDC AE44 Alloy, *Adv. Eng. Mater.*, 2016, **18**, p 148–155
26. M.P. Liu, Q.D. Wang, Z.L. Liu, G.Y. Yuan, G.H. Wu, Y.P. Zhu, and W.J. Ding, Behavior of Mg-Al-Ca Alloy During Solution Heat Treatment at 415 °C, *J. Mater. Sci. Lett.*, 2002, **21**, p 1281–1283
27. B. Hu, L.M. Peng, Y.L. Yang, and W.J. Ding, Effect of Solidification Conditions on Microstructure, Mechanical and Wear Properties of Mg-5Al-3Ca-0.12Sr Magnesium Alloy, *Mater. Des.*, 2010, **31**(8), p 3901–3907
28. L. Wang, Y.C. Feng, L.P. Wang, Y.H. Chen, and E.J. Guo, Effect of Al on Grain Refinement and Mechanical Properties of Mg-3Nd Casting Alloy, *J. Mater. Eng. Perform.*, 2018, **27**, p 1–11
29. P.H. Fu, L.M. Peng, H.Y. Jiang, Z.Y. Zhang, and C.Q. Zhai, Fracture Behavior and Mechanical Properties of Mg-4Y-2Nd-1Gd-0.4Zr (wt.%) Alloy at Room Temperature, *Mat. Sci. Eng. A*, 2008, **486**, p 572–579